Desalination and Water Treatment
www.deswater.com

doi: 10.1080/19443994.2015.1106351

57 (2016) 19834–19845
September

Taylor & Francis
Taylor & Francis Group

Application of thiol-functionalized mesoporous silica-coated magnetite nanoparticles for the adsorption of heavy metals

Mahsa Tahergorabi, Ali Esrafili*, Majid Kermani, Mehdi Shirzad-Siboni

Department of Environmental Health Engineering School of Public Health, Iran University of Medical Sciences, Tehran, Iran, Tel. +98 9124359726, emails: tahergurabi.m@tak.iums.ac.ir, nahal_parsa@yahoo.com (M. Tahergorabi), Tel. +98 9124976672, +98 9122588677; Fax: +98 2188607939; email: a_esrafily@yahoo.com (A.Esrafili), Tel. +98 9122250387; email: majidkermani@yahoo.com (M. Kermani), Tel. +98 9112346428; emails: mshirzadsiboni@yahoo.com, shirzad.m@iums.ac.ir (M. Shirzad-Siboni)

Received 31 May 2015; Accepted 25 September 2015

ABSTRACT

This study investigated the removal of heavy metals such as Ni(II), Cu(II), and Cr(III) in aqueous solutions by the synthesis of thiol-functionalized mesoporous silica-coated magnetite nanoparticles (TF-SCMNPs) with different pH levels, contact times, and adsorbent dosages. The synthesis of TF-SCMNPs samples occurred with simple co-precipitation methods. FT-IR, X-ray diffraction, SEM, energy dispersive X-ray, and VSM techniques were used for characterization of the prepared adsorbent. The removal efficiency of heavy metals by TF-SCMNPs was more than that of magnetite in similar conditions. The results showed that the maximum adsorption of TF-SCMNPs for Ni(II), Cu(II), and Cr(III) was obtained at pH 7, 10, and 10 during the contact time of 20 min, respectively. By increasing adsorption dosage the removal efficiency was increased. The study of the adsorption kinetic model revealed that the pseudo-second-order model was the best applicable one to describe the adsorption of Ni(II) and Cu(II), pseudo-first-order model for Cr(III)onto TF-SCMNPs. Adsorption data were analyzed by both Langmuir and Freundlich adsorption isotherms and the results showed that it was better described by the Langmuir model for Ni(II), Cu (II), and Freundlich model for Cr(III). The maximum adsorption capacities were estimated to be 4.476, 4.038, and 1.119 mg/g at optimum pH and room temperature for Cu(II), Ni(II), and Cr(III), respectively. TF-SCMNPs nanoparticles were maintained even after five successive cycles, suggesting a promising adsorbent for aquatic-contaminated heavy metals.

Keywords: Heavy metals; TF-SCMNPs nanoparticle; Kinetic and Isotherm models; Adsorption; Aqueous solutions

1. Introduction

The most important natural resource for the human survival in the world is water [1]. Population growth and industrialization are the main causes for aquatic pollution [1]. The most important pollutants of environment are heavy metals [1,2]. Heavy metals such as Cu(II), Ni(II), and Cr(III) may cause poisoning, diseases, and even death for aquatic organisms and human [3–5]. Toxicity level of heavy metals depends on the type of metal, biological role, and the type of organisms that are exposed to it [3]. The known fatal

*Corresponding author.

effects of heavy metal toxicity in water resources include mental disorder, damaged central nervous system, and lower energy level [6]. The long-term exposure of these metals results in physical, muscular, severe neurological diseases such as Alzheimer's disease (brain disorder), Parkinson's disease(destructor disease of the brain), muscular (advanced skeletal muscle weakness), and multiple sclerosis (a nervous system disease that affects brain and spinal cord) [6]. Water and wastewater pollutants mainly consist of heavy metals, micro-organisms, fertilizers, and thousands of toxic organic compounds [7]. As trace elements, some heavy metals (e.g. copper, selenium, zinc) are essential to maintain the metabolism of the human body [8]. However, at higher concentrations, they may lead to poisoning individuals, since they tend to bioaccumulate in the human body [8]. Ingesting amounts of Cu(II), Ni(II), and Cr(III) can cause death by nervous system, liver, and kidney failure [8]. Maximum contaminant level (MCL) in drinking water is equal to (0.1 mg/L) and (0.05 mg/L) for copper, (0.05–0.005 mg/L) and (0.2 mg/L) for nickel, and (0.05 mg/L) and (0.05 mg/L) for chromium, according to WHO and USEPA guidelines, respectively. The most commonly used procedures for removing metal ions from aqueous solution include adsorption, chemical precipitation, lime, coagulation, ion exchange, reverse osmosis, electro dialysis, and solvent extraction [9–11]. The disadvantage of coagulation–flocculation is the high operational cost due to chemical consumption [9]. The disadvantage of ion exchange is that it cannot be applied to concentrated metal solution as the matrix gets easily fouled by organics matter and other solids in the water [9]. Moreover, ion exchange is nonselective and is highly sensitive to the pH of the solution [9]. The disadvantage of electro dialysis is the formation of metal hydroxides, which clog the membrane [9]. The disadvantage of membrane filtration is high operational cost due to membrane fouling [9]. Among them, adsorption technique has attracted more attention because it is simple, efficient, and requires low operating cost. When adsorption capacity of the used adsorbents has been exhausted, they should be separated from the aquatic system using filtration method and regenerated [12]. However, filtration is a tedious process causing blockage in filters [12]. Recently magnetic separation has much attention as a promising environmental technique since it produces no contaminants and has the ability to treat large amount of wastewater within a short span of time. Fe_3O_4 is a traditional magnetic material having superparamagnetic property [13,14]. It can be recovered very quickly by external magnetic field and reused without losing the active site [13]. To protect magnetic nanoparticles from oxidation or being dissolved under low pH conditions, thiol is good modify functionalize to coat magnetic nanoparticles with silica shell which owner reliable chemical stability, biocompatibility and versatility in surface modification [15]. Thiol group is organic ligand and strong resemble with heavy metal ions according to Pearson's hard soft acid–base theory [15]. Shen et al. reported removal efficiencies of 97.6, 99.8, and 88.5% for Cr(VI), Cu(II), and Ni(II) by adsorption onto Fe_3O_4, respectively [16]. Liu et al. reported removal efficiencies of 92.4, 50.4, and 46.3% for Pb(II),Cd(II), and Cu (II) by Fe_3O_4–Humic acid, respectively [17]. Yantasee et al. reported removal efficiency of 99% for Pb(II) by adsorption with Fe_3O_4-modified SH [18].

In this study, thiol-functionalized mesoporous silica-coated magnetite nanoparticles (SCMNPs) was used for the adsorption of heavy metals such as Cu (II), Ni(II), and Cr(III) from aqueous solutions. The effects of pH and adsorbent dosage in different time intervals on the removal efficiency were studied. Adsorption kinetic and isotherm studies were undertaken to comprehend the adsorption mechanism and maximum adsorption capacity of SCMNPs nanoparticles.

2. Materials and methods

2.1. Chemicals

$FeCL_3{\cdot}6H_2O$, $FeCl_2{\cdot}6H_2O$, 3-mercaptopropyltrimethoxysilane (3-MPTS), and ethanol (EtOH), copper nitrate, nickel nitrate, chrome nitrate, which were of analytical grade, were purchased from Merck, Germany and used without any purification. The initial pH of the solution was adjusted by the addition of 0.1 M NaOH or HCl, and measured by pH meter (Metron, Switzerland). The experiments were carried out at room temperature (25 ± 2˚C). Heavy metal stock solutions (1,000 mg/L) were prepared with appropriate amount of heavy metal salts in distilled water and kept in dark.

2.2. Synthesis of TF-SCMNPs nanoparticles

TF-SCMNPs nanoparticles were prepared via the co-precipitation method in alkaline solution [15]. This preparation includes three stages (Fe_3O_4, Fe_3O_4@$nSiO_2$, and TF-SCMNPs). Fe_3O_4 was prepared using the co-precipitation method described in pervious works [16]. The appropriate amount of $FeCl_3{\cdot}6H_2O$ and $FeCl_2{\cdot}4H_2O$ were dissolved in 200 mL deionized water. NH_4OH 25% (25 mL) was added dropwise to the precursor solution to obtain an alkaline medium

(pH 8) producing a black and gelatinous precipitate of Fe_3O_4 nanoparticles under nitrogen gas. It was heated at 80˚C for 2 h with continuous stirring. The desired Fe_3O_4 nanoparticles were collected by a permanent magnet and then washed with deionized water and ethanol for five times. Then, it was dried at 80˚C in vacuum for 5 h. Then, appropriate amount of the TEOS, ethanol, and NH_3 were added to the previous stage to obtain Fe_3O_4@nSiO_2 under nitrogen gas and mixed for 2 h. TF-SCMNPs nanoparticles were prepared via adding appropriate amount of the MPTMS, TEOS, ethanol, and NH_3 to previous stage nitrogen gas and mixed for 24 h. The desired TF-SCMNPs nanoparticles were collected by a permanent magnet and then washed with deionized water and ethanol for five times. Then it was dried at 80˚C in vacuum for 5 h. The point of zero charge (pH_{pzc}) was determined to investigate the surface charge properties of the adsorbents. The pH_{ZPC} of TF-SCMNPs nanoparticles was determined adopting the method previously used [19]. For characterization of the functional groups on the surface of the samples, Fourier transform infrared spectroscopy (FT-IR) spectra were recorded using a Perkin-Elmer (Germany) spectrometer under dry air at room temperature by the KBr pellets method. The spectra were collected over the range from 400 to 4,000 cm^{-1}. The X-ray diffraction (XRD) studies were performed with a Philips XRD instrument (Siemens D-5000, Germany) using Cu Kα radiation (λ = 1.5406 Å) at wide-angle range (2θ value 4˚–80˚) at 40 kV of accelerating voltage and at 30 mA of emission current. The surface morphology of Fe_3O_4 and TF-SCMNPs nanoparticles was obtained by a field emission scanning electron microscopy (Mira3, Tescan, Czech Republic). SEM images were further supported by energy dispersive X-ray (EDX) to provide direct evidence for the purity, existence, and distribution of specific elements in a solid sample. The magnetic property of TF-SCMNPs nanoparticles was characterized by vibrating Sample Magnetometer (VSM, MDKFD, Iran).

2.3. Adsorption experiments

The adsorption experiments were carried out in 1,000 mL Erlenmeyer flask containing 100 mL of Ni(II), Cu(II), and Cr(III) solution and 0.04 g/100 mL, while the mixtures were stirred at 150 rpm and room temperature (25 ± 2˚C) in different time intervals (5–20 min). Then adsorbent was separated from the mixture solution by permanent magnet. The residual concentration of the Ni(II), Cu(II), and Cr(III) in each sample was measured using a flame atomic adsorption spectrophotometer (Analyst 200-perkinelmer) [20]. In order to determine the effects of various parameters, the experiments were conducted at different adsorbent amounts of 0.008–0.04 g/100 mL, and initial pH of 3–10. Each experiment was conducted in triplicates and mean values of data were reported. The removed amount of heavy metals by TF-SCMNPs nanoparticles and the removal efficiency were calculated by Eqs. (1) and (2), respectively [19]:

$$q = \frac{(C_0 - C_e)V}{M} \times 100 \quad (1)$$

$$\text{Removal efficiency}\,(\%) = \frac{(C_i - C_0)}{C_i} \times 100 \quad (2)$$

where q is the adsorption capacity (mg/g), C_i, C_0, and C_e are the initial, outlet, and equilibrium concentrations of dye (mg/L), respectively, V is the volume of the dye solution (L), and M is the total amount of TF-SCMNPs nanoparticles (g) [19].

3. Results and discussion

3.1. Adsorbent characterization

3.1.1. FT-IR analysis

FT-IR analysis of Fe_3O_4 and TF-SCMNPs nanocomposite were performed in the range of 400–4,000 cm^{-1} Fig. 1. Fe_3O_4 nanoparticles showed significant absorption peaks at 447, 580, 860, 1,403, 1,623, 3,378, 3,788, and 3,850 cm^{-1}. TF-SCMNPs nanoparticles showed significant absorption peaks at 461.83, 593.04, 802.37, 1,081.22, 1,429.30, 1,545.40, 1,711.56, 2,360.25, 2,852.33, 2,922.20, 3,366.80, 3,743.08, and 3,857.20 cm^{-1}. The two distinct absorption peaks at 580 and 447 cm^{-1} are attributed to the vibrations of Fe^{3+}–O^{2-} and Fe^{2+}–O^{2-}, respectively [15,21]. Moreover, for TF-SCMNPs, the peak at ~802.37 cm^{-1} is attributed to the vibration of aromatic Si–C bonding, and the peak at ~2,360.25 cm^{-1} is attributed to the vibration of aromatic S–H bonding [15,21]. The peak at ~2,852.33 cm^{-1} is assigned to an aromatic C–H and O–CH_3 stretching [15,21]. The FT-IR analysis supported good thiol-functionalized mesoporous silica-coated magnetite nanoparticles.

3.1.2. XRD analysis

The XRD patterns of Fe_3O_4 and TF-SCMNPs nanoparticles are illustrated in Fig. 2. The patterns exhibit crystalline structure of both Fe_3O_4 and TF-SCMNPs nanoparticles even after thiol-functionalized mesoporous silica-coated magnetite nanoparticles. The main peaks at 2θ values of 18.27, 21.16, 30.11, 30.21,

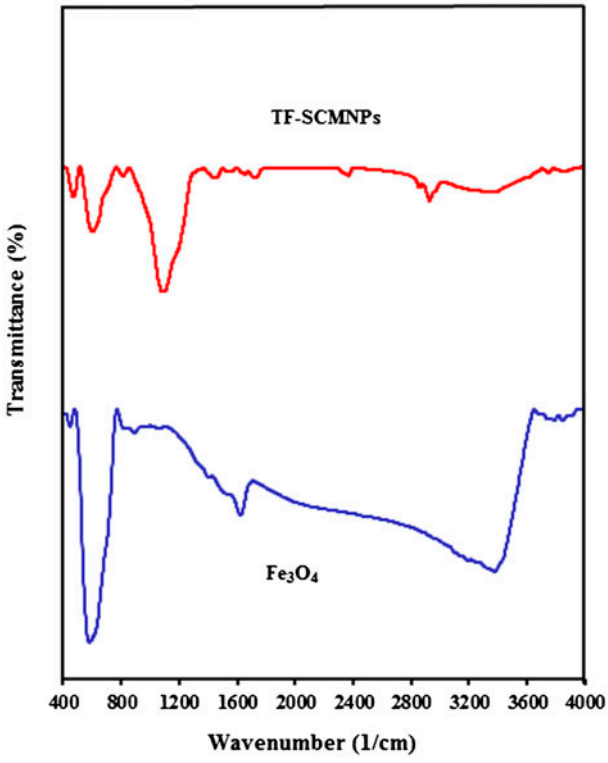

Fig. 1. FT-IR spectra of samples.

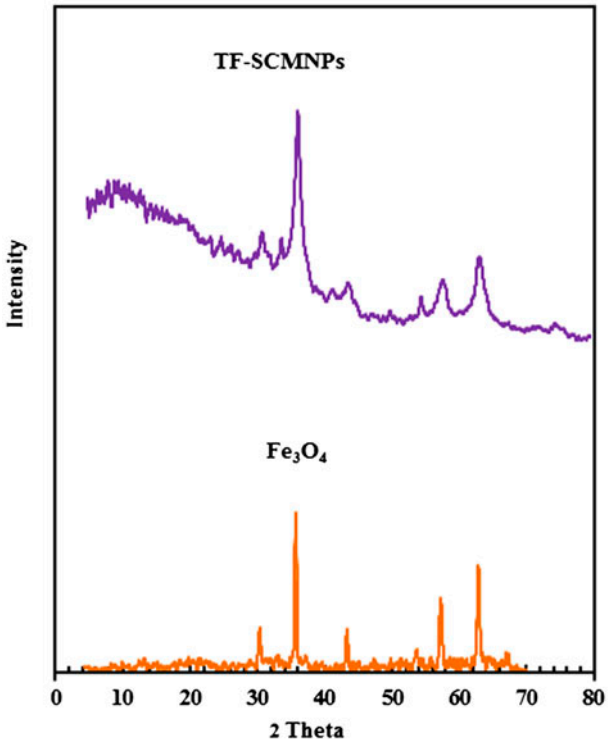

Fig. 2. Typical XRD patterns of samples.

35.42, 35.53, 37.03, 37.18, 43.12, and 57.09 correspond to the (0 1 1), (0 0 2), (1 1 2), (2 0 0), (1 2 1), (1 0 3), (0 2 2), (2 0 2), (0 0 4), and (3 2 1) planes of orthorhombicFe_3O_4 (JCPDS card no. 031156). As illustrated in Fig. 3, the peaks related to the Fe_3O_4 nanoparticles are still observed after the thiol-functionalized mesoporous silica-coated magnetite nanoparticles. The average crystalline size of Fe_3O_4 and TF-SCMNPs nanoparticles were calculated using the following Debye–Sherrer's equation (Eq. (3)) [22]:

$$D = \frac{0.9\lambda}{\beta \cos \theta} \tag{3}$$

where D is the average crystallite size (Å), λ is the wavelength of the X-ray radiation (Cu Kα = 1.54178 Å), β is the full width at half maximum intensity of the peak, and θ is the diffraction angle. According to the Eq. (3), the mean crystallite size of the Fe_3O_4 and TF-SCMNPs nanoparticles were estimated to be 8 and 11 nm, respectively.

3.1.3. SEM and EDX analyses

SEM images of Fe_3O_4 and TF-SCMNPs nanoparticles are shown in Fig. 3(a) and (b), respectively. Fig. 3(b) clearly illustrates the distribution of thiol-functionalized mesoporous silica over the surface of the magnetite nanoparticles. The size of TF-SCMNPs nanoparticles was around 10 nm. Li et al. reported the average diameter of the particles around 500 nm for SH-mSi@Fe_3O_4 [15]. Also, they are reported the average pore diameter equal to 2.5 nm. The BET area and total pore volume were calculated to be 321 m^2/g and 0.29 cm^3/g, respectively [15].

EDX microanalysis was used to characterize the elemental composition of the Fe_3O_4 and TF-SCMNPs nanoparticles. EDX pattern of the Fe_3O_4 and TF-SCMNPs nanoparticles are depicted in Fig. 4. According to the EDX analysis, the major elements were Fe (57.63%), O (29.18%), Si (5.88%), and S (3.15%) indicating good hybridization thiol-functionalized mesoporous silica-coated magnetite nanoparticles. Li et al. reported the element mass contents of Si, S, and Fe in SH-mSi@Fe_3O_4 equal to 17.95, 1.23, and 38.03%, respectively [15]. VSM was used to measure magnetite property of Fe_3O_4 and TF-SCMNPs. VSM magnetization curve of the Fe_3O_4 and TF-SCMNPs nanoparticles at room temperature is depicted in Fig. 5. The saturated magnetization value of Fe_3O_4 and TF-SCMNPs nanoparticles was 58.97 and 32.43 μ/g, respectively. These results also indicated that the TF-SCMNPs nanoparticles showed an excellent

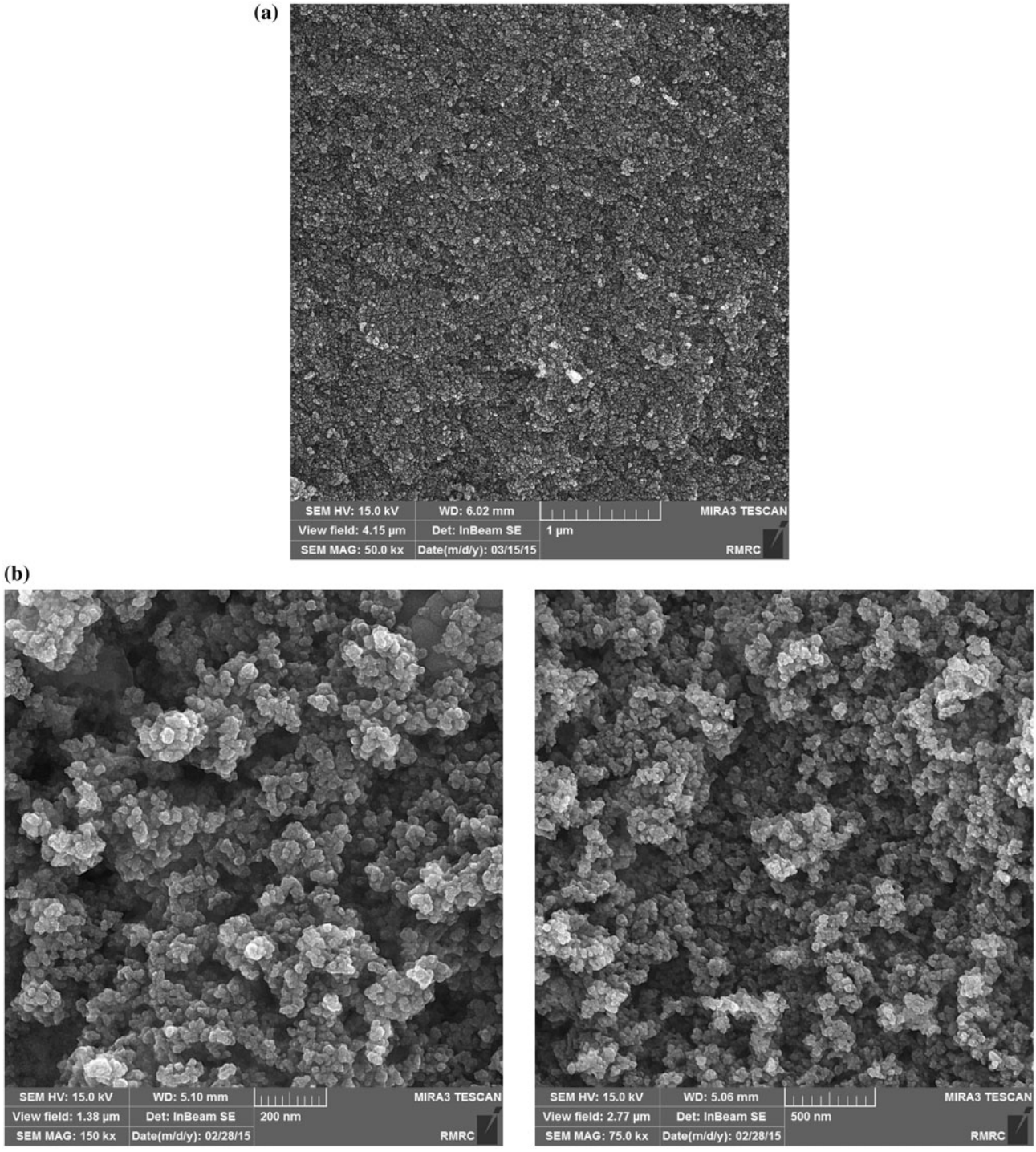

Fig. 3. SEM image of samples (a) Fe_3O_4 nanoparticles and (b) TF-SCMNPs nanoparticles.

magnetic response to a magnetic field. Therefore, it could be separated easily and rapidly due to this high magnetic sensitivity. This value is smaller than the magnetization value of amino-functionalized Fe_3O_4-SiO_2 (34.0 μ/g) [23], and greater than thiol-functionalized superparamagnetic carbon nanotubes (29.02 μ/g) reported by other researchers [24]. Zhang et al. reported that the maximal saturation magnetization of Fe_3O_4, Fe_3O_4@SiO_2, and Fe_3O_4@SiO_2–SH were 55.05, 25.45, and 20.47 μ/g, respectively [25].

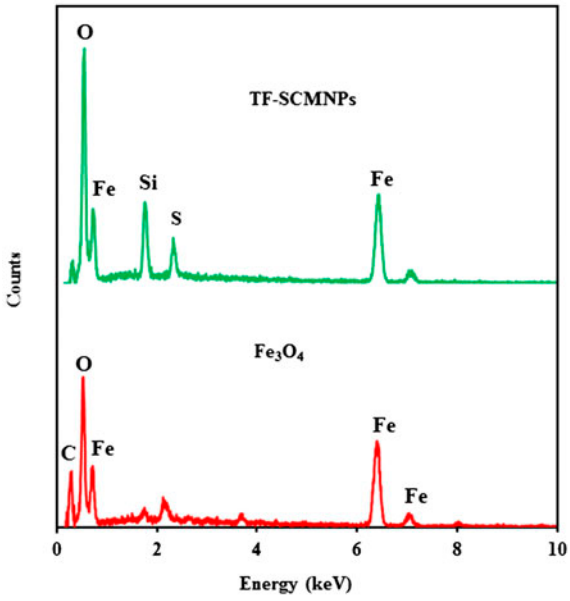

Fig. 4. EDX image of samples.

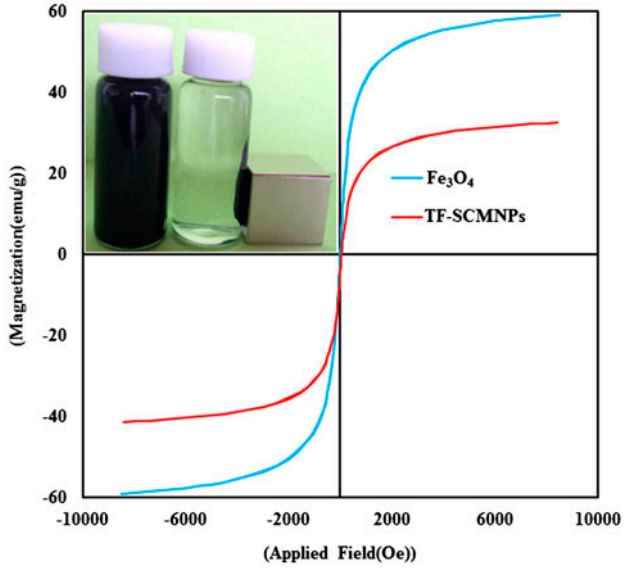

Fig. 5. VSM image of samples.

3.2. Effect of parameters on the removal of heavy metals with TF-SCMNPs nanoparticles

3.2.1. Effect of Solution pH and contact time

The effect of initial pH on the removal of heavy metals on the TF-SCMNPs nanoparticles was investigated by varying the initial pH from 3 to 10 and at constant condition (Cu(II) and Ni(II) = 2 mg/L and Cr(III) = 8 mg/L, adsorbent dose = 0.04 g/100 CC) in different time intervals (Fig. 6). As shown in Fig. 7, with increasing the initial pH from 3 to 10 at different time intervals, the removal efficiency Cr(III) and Cu(II) increased, but decreased for Ni(II). According to the data, the pHzpc of TF-SCMNPs nanoparticles is 6. This means that at pH values below 6, the TF-SCMNPs surface has a net positive charge, while at pH greater than 6, the surface has a net negative charge [26]. At pH values above pH of point of zero charge (pH_{zpc}), adsorption of Cu, Ni, and Cr was complete, although increasing amount of metal ions could be adsorbed at relatively higher pH [26]. The metal cations have tendency to hydrate in aqueous solution with the increase in the pH value, thus resulting in increased adsorption during adsorbate/adsorbent interaction with the increase in the pH value [26]. The decrease in adsorption with decreasing solution pH is in that way attributed to low mobility hydrated species, competition of H^+ for available surface sites, and the reinforcement protonation of the –SH group in acidic condition [26]. To compare magnetic nanoparticles and TF-SCMNPs for removal Ni(II) included that with increasing pH from 2 to 8 removal efficiency Ni(II) for both adsorbent increased. Maximum uptake of Ni(II) ions took place at pH 8 with 99.2% for the concentrations of 25 Ni^{2+} mg/L [13]. These results are in agreement with our obtained results. As shown in Fig. 6 with increasing contact time from 5 to 20 min, the removal efficiency increases from 2.5 to 42% for Cr(III), 45.5 to 96.3% for Cu(II), and 32 to 93.5% for Ni (III), respectively. As shown in Fig. 6, the removal rate of Ni(II), Cu(II), and Cr(III) at

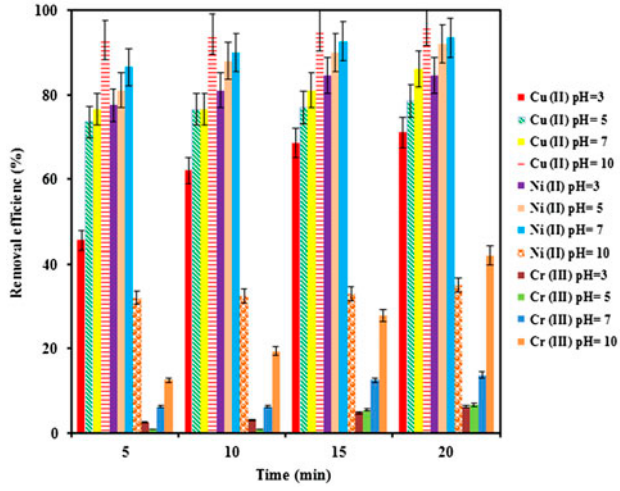

Fig. 6. Effect of pH on the removal of heavy metals by TF-SCMNPs nanoparticles in different time interval (Cu(II) and Ni(II) = 2 mg/L and Cr(III) = 8 mg/L, adsorbent dose = 0.04 g/100 CC).

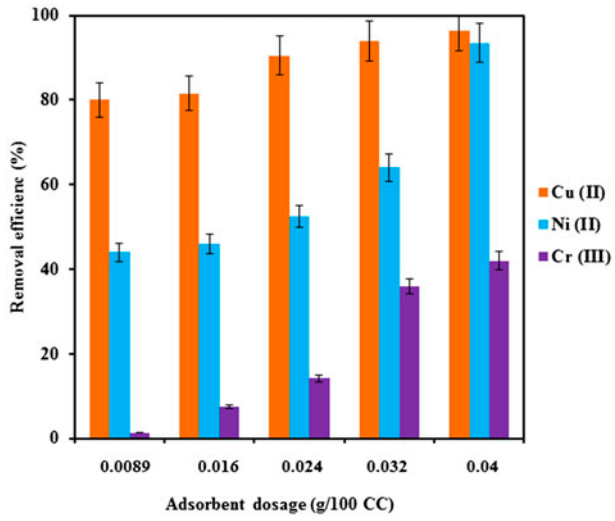

Fig. 7. Effect of adsorbent dose on the removal of heavy metals by TF-SCMNPs nanoparticles (Cu(II) and Ni(II) = 2 mg/L and Cr(III) = 8 mg/L, Time = 20 min pH 10 for Cu(II) and Cr(III) and pH 7 for Ni(II)).

all dosages was rapid in the first stages of contact time (5 min), and then it was gradually slowed until reactions reached a near equilibrium after 20 min. Kumari et al. reported the removal efficiency equal to 44% at contact time equal to 60 min with magnetic nanoparticles, and 93.5 and 96.3% with TF-SCMNPs at contact time equal to 20 min for Ni(II) and Cu(II), respectively [13,27]. Also, the stability of TF-SCMNPs nanoparticles has been assessed at different solution pH values. According to the pHzpc data, the results showed that TF-SCMNPs nanoparticles are stable in acidic solutions (pH > 2). The results showed that the most removal of TF-SCMNPs for Ni(II), Cu(II), and Cr(III) was obtained at pH 7, 10, and 10 in contact time 20 min, respectively. The other experiments were performed at this pHs.

3.2.2. Effect of adsorbent dosage

The effect of adsorbent dosage on the removal of heavy metals on the TF-SCMNPs nanoparticles was investigated by varying the initial adsorbent dosage from 0.008 to 0.04 g/100 mL and at constant condition Cu(II) and Ni(II) = 2 mg/L and Cr(III) = 8 mg/L, adsorbent dose = 0.04 g/100 CC, Time = 20 min) (Fig. 7). As shown in Fig. 7 with increasing adsorbent dosage from 08 to 0.04 g/100 mL, the removal efficiency of Cr(III), Cu(II), and Ni(II) increased from 1.375 to 42%, 80 to 96.3%, and 44 to 93.5%, respectively. This trend can be explained by the increased active sites for the removal of contaminants along with the increase in the adsorbent dosage. Similar observations were also reported for the removal of heavy metals by magnetite and TF-SCMNPs nanoparticles [28–30].

3.2.3. Comparison of each process

To evaluate the effect of various processes on the removal efficiency of Cu(II), Cr(III), and Ni(II) by Fe_3O_4 and TF-SCMNPs nanoparticles, they were compared under constant conditions (Cu(II) and Ni(II) = 2 mg/L and Cr(III) = 8 mg/L, adsorbent dose = 0.04 g/100 CC, Time = 20 min, TF-SCMNPs and Fe_3O_4 = 0.04 g/100 mL and pH 10, 10, and 7) (Fig. 8). Fig. 8 shows that the removal efficiency of Ni (II), Cu(II), and Cr(III) with TF-SCMNPs nanoparticles was 93.5, 96.3, and 42% and with Fe_3O_4 nanoparticles 40, 50.55 and 13.875%, respectively [13,27]. These experiments demonstrate that TF-SCMNPs nanoparticles are needed for the effective removal of heavy metals. Reusability of adsorbent is an important factor for the application of developed adsorbent in the treatment of water and wastewater [26]. Hence, the adsorption of Ni(II), Cu(II), and Cr(III) was performed by TF-SCMNPs nanoparticles for four repeated runs with HCl and without it. As can be seen in Fig. 9, the adsorption capacity of Ni(II), Cu(II), and Cr(III) by TF-SCMNPs nanoparticles was reduced to four consecutive runs.

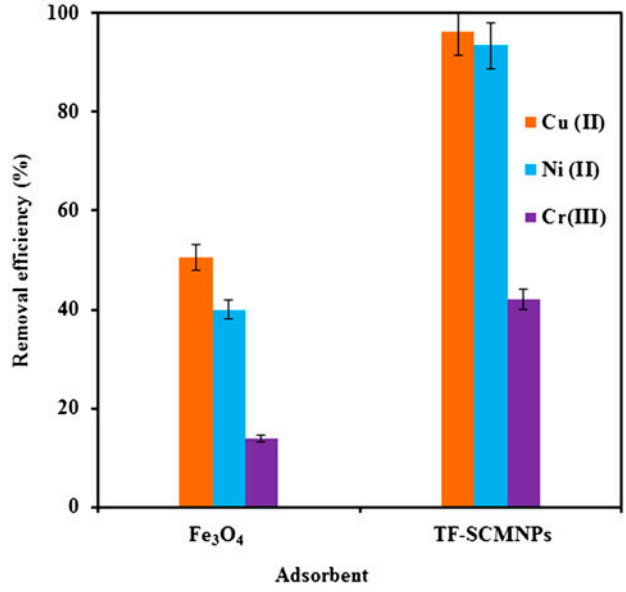

Fig. 8. Results of reusability test for the removal of heavy metals by TF-SCMNPs nanoparticles (Cu(II) and Ni(II) = 2 mg/L and Cr(III) = 8 mg/L, Time = 20 min pH 10 for Cu(II) and Cr(III) and pH 7 for Ni(II)).

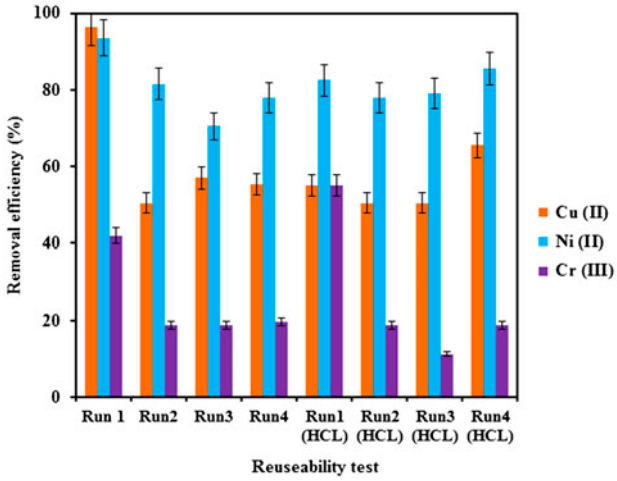

Fig. 9. Contribution of each process involved on the removal of heavy metals by TF-SCMNPs nanoparticles (Cu (II) and Ni(II) = 2 mg/L and Cr(III) = 8 mg/L, Time = 20 - min pH 10 for Cu(II) and Cr(III) and pH 7 for Ni(II)).

3.3. Kinetic, equilibrium, and thermodynamic studies

Adsorption kinetic experiments were performed at initial Ni(II), Cu(II), and Cr(III) concentration (2, 2, and 8 mg/L), at constant adsorbent dosage (0.04 g/100 mL) and at pH 7, 10, and 10. The pseudo-first-order, pseudo-second-order and intra-particle diffusion model models were applied in order to find an efficient model for the description of adsorption. The relevant equations for the kinetic and equilibrium studies are shown in Table 1 [13,19,31–35]. To obtain kinetic data for the removal of heavy metals, ln $(1 - q_t/q_e)$ and t/q_2 vs. t and q_t vs. $t^{0.5}$ was plotted for the pseudo-first-order, pseudo-second-order, and intra-particle diffusion models, respectively. The kinetic parameters for the removal of Ni(II), Cu(II), and Cr(III) at different pH by pseudo-first-order, pseudo-second-order, and intra-particle diffusion models are summarized in Table 2. The study of the adsorption kinetic model revealed that the pseudo-second-order model was the best applicable one to describe the adsorption of Ni(II) and Cu(II) (R^2 = 0.9994 and 0.9998), pseudo-first-order model for Cr(III) (R^2 = 0.9975) onto TF-SCMNPs. The estimated P values for Ni(II), Cu(II), and Cr(III) have been summarized in Table 2. From these results, it is inferred that the kinetic data for Ni(II), Cu(II), and Cr(III) adsorption fitted well with both the pseudo-second-order model and pseudo-first-order ($p < 0.05$), in comparison to another kinetic models. To investigate the adsorption equilibrium isotherm, experiments were performed with various adsorbent dosages (0.008–0.04 g/100 mL) at pH (7, 10, 10) for 24 h. All experiments were repeated three times and the average values were reported. Langmuir and Freundlich equations were applied to fit experimental adsorption data, and the related equations are shows in Table 1 [13,19,31–33,36]. R_L value (separation factor) expresses a characteristic of the Langmuir isotherm. Generally, adsorption will be favorable when R_L value is between 0 and 1, while unfavorable adsorption will be expected at R_L value above 1 e, R_L values 1 and 0 correspond to linear and irreversible adsorptions, respectively. The values of q_m and k_L for each heavy metal are given in Table 3. The removal capacity of Cr(III), Cu(II), and Ni(II) by TF-SCMNPs nanoparticles was compared with that by other adsorbents in Table 3. Adsorption data showed that it was better described by the Langmuir model for Ni(II) and Cu(II) and Freundlich model for Cr(III). The maximum adsorption capacity was estimated to be 4.476, 4.038, and 1.119 mg/g at optimum pH and room temperature for Cu(II), Ni(II), and Cr(III), respectively. Also, separation factor (R_L) was calculated as 0.064–0.125, 0.96–0.98, and 0.0007–0.001, for Ni(II), Cu(II), and

Table 1
Kinetic and isotherm and thermodynamic equations for adsorption of heavy metals by with TF-SCMNPs nanoparticles

Kinetic models	Isotherm equations	Parameters
Pseudo-first-order $\ln\left(1-\frac{q_t}{q_e}\right) = -k_1 t$	Freundlich isotherm $\log q_e = \log K_F + \frac{1}{n}\log C_e$	q_e (mg/g), q_t (mg/g), k_1 (1/min), k_2 (g/mgmin), K_L (L/mg), q_m (mg/g), K_F ($mg^{1-1/n}\ L^{1/n}\ g^{-1}$, K_p ($mg/g \cdot min^{-0.5}$), C_0 (mg/g)
Pseudo-second-order $\frac{t}{q_t} = \frac{1}{k_2 q_e^2} + \frac{1}{q_e} t$	Langmuir isotherm $q_e = \frac{K_L q_m C_e}{1 + K_L C_e}$	
Intra-particle diffusion model $q_t = K_p \times t^{0.5} + C$		

Table 2
Calculated kinetic parameters for pseudo-first-order, pseudo-second-order and intra-particle diffusion models for removal of heavy metals by with TF-SCMNPs nanoparticles

	Pseudo-first-order model					Pseudo-second-order model				Intra-particle diffusion model			
pH	$q_{e(exp)}$ (mg/g)	k_1 (1/min)	$q_{e(cal)}$ (mg/g)	R^2	p-value	k_2 (g/mgmin)	$q_{e(exp)}$ (mg/g)	R^2	p-value	K_p (mg/g·min$^{-0.5}$)	C_0 (mg/g)	R^2	p-value
Cu(II)													
3	3.55	0.121	3.8	0.9812	0.009	0.182	3.717	0.9779	0.001	0.575	1.1117	0.9301	0.036
5	3.925	0.0911	4	0.9524	0.024	1.349	3.93	0.9996	0.000	0.106	3.4546	0.9467	0.027
7	4.3	0.0811	4.5	0.8333	0.087	0.474	4.273	0.9952	0.003	0.2125	3.2699	0.8162	0.097
10	4.815	0.0417	5	0.9931	0.03	1.839	4.81	0.9998	0.000	0.0724	4.486	0.9951	0.002
Ni(II)													
3	4.225	0.0798	4.4	0.8992	0.052	0.87	4.264	0.9991	0.000	0.1683	3.5154	0.935	0.033
5	4.6	0.067	4.9	0.9628	0.019	0.591	4.631	0.9986	0.000	0.2414	3.5581	0.9422	0.029
7	4.675	0.0009	4.8	0.9446	0.028	0.882	4.699	0.9994	0.00	0.1608	3.9792	0.9791	0.011
10	1.75	0.0296	2	0.8329	0.087	1.704	1.734	0.9973	0.002	0.0613	1.4455	0.8061	0.102
Cr(III)													
3	1.25	0.0925	1.5	0.9088	0.047	0.143	1.323	0.7385	0.226	0.3381	0.3305	0.9298	0.036
5	1.35	0.2725	1.37	0.8590	0.074	0.0059	3.4	0.0344	0.16	0.5688	1.2169	0.9055	0.048
7	2.75	0.1306	3	0.9975	0.001	0.096	3.022	0.8923	0.002	0.682	0.2184	0.9851	0.007
10	8.4	0.2138	8.6	0.766		0.0143	9.149	0.6028		2.5442	3.6602	0.9296	
10	118.87	0.0348	119	0.7559	0.125	0.0022	117.64	0.9947	0.469	7.445	50.157	0.6688	0.036

Table 3
Isotherm constants for the adsorption of heavy metals by with TF-SCMNPs nanoparticles

Adsorbents	Heavy metals	Freundlich constants			Langmuir constants			Refs.
		K_F ($mg^{1-1/n}$ $L^{1/n}$ g^{-1})	n	R^2	q_m (mg/g)	K_L (L/mg)	R^2	
Fe_3O_4/MnO_2	Cu(II)	–	–	–	9.84	0.392	0.996	[9]
Grafted Silica	Cu(II)	–	–	–	0.0566	9.10	0.961	[28]
Activated Carbon	Cu(II)	–	–	–	0.18	0.24	0.85	[30]
Sawdust	Ni(II)	7.87	4.2	0.9734	22.47	0.17	0.9937	[32]
Charcoal Ash	Ni(II)	0.363	0.84	0.98	33.22	0.013	0.99	[42]
Rice Husk	Cu(II)	–	–	–	31.85	–	–	[43]
Montmorillonite	Ni(II)	3.40	0.53	0.99	21.14	137.74	0.99	[43]
Bentonite	Cu(II)	1.622	0.540	0.9803	14.104	0.075	0.9804	[43]
Chitosan/Magnetite	Ni(II)	–	–	–	23.30	0.5939	0.977	[44]
Tree Fern	Cu(II)	3.24	0.261	0.818	10.6	0.134	0.998	[45]
Red Mud	Ni(II)	0.289	0.532	0.999	10.95	7.193	0.986	[46]
Red Mud	Cu(II)	0.122	0.627	0.991	19.7	2.029×10^1	0.905	[46]
Kaolinite	Ni(II)	0.94	0.49	0.99	7.05	70.14	0.99	[47]
Natural Chitosan	Cu(II)	–	–	–	2.0 ± 0.1	14.1 ± 2.5	0.96	[48]
Prawn Shell	Cu(II)	–	–	–	0.236	0.254	0.978	[49]
Kaolinite	Ni(II)	–	–	–	1.669	0.112	–	[49]
Clinoptilolite	Ni(II)	0.676	0.553	0.911	3.28	0.182	0.996	[50]
TF-SCMNPs	Cu(II)	4.184	18.38	0.9889	4.476	186.16	0.9999	This study
TF-SCMNPs	Ni(II)	3.773	9.398	0.9885	4.038	53.82	0.9996	This study
TF-SCMNPs	Cr(III)	678.42	0.355	0.9435	1.119	0.238	0.8746	This study

Cr(III), respectively. The values of heavy metals uptake found in this work are higher than the other reported values; for example q_m (mg/g) is 1.31 for the removal of Hg and q_m (mg/g) is 0.442 for the removal of Pb onto SH-mSi@Fe_3O_4 [15], q_m (mg/g) is 1.29 for mercury adsorption onto Fe_3O_4@-SiO_2–SH [25], q_m (mmol/g) is 2.26 for the removal of Cu(II) onto amphoteric functionalized mesoporous silica (AG-SBA-15) [37], q_m (mmol/g) is 0.47, 0.37, and 0.2 mg/g for Cu^{2+}, Pb^{2+}, and Cd^{2+} onto Fe_3O_4@-SiO_2–NH_2 [23]. Also lower than other reported papers; for example q_m (mg/g) is 32.58 and 16.50 for the removal of Pb(II) onto Fe_3O_4@ SiO_2-IIP and Fe_3O_4@ SiO_2-NIP, respectively [38], q_m (mg/g) is 130 and 39 for Pb^{2+} and Cd^{2+} onto thiol-functionalized silica (HBS-SH) [39], q_m (mg/g) is 182, 147, and 141 for Cu^{2+}, Zn^{2+}, and Cd^{2+} onto OSU-6-W-TCSPBr-2-TEPA [40]. q_m (mg/g) is 193.85 for Cr(VI) onto PANI–magnetic mesoporous silica [41]. This comparison of sorption capacity of TF-SCMNPs nanoparticles used in this study with those obtained in the literature shows that the TF-SCMNPs nanoparticles are an effective adsorbent for the removal of heavy metals from aqueous solution.

4. Conclusion

In this research, application of TF-SCMNPs nanoparticles for the adsorption of heavy metals in aqueous solutions was studied. The prepared sample was characterized by of FT-IR, XRD, SEM, EDX, and VSM Analysis. XRD analysis showed crystallized nature of Fe_3O_4 with pure orthorhombic phase. The removal efficiency depended on experimental parameters like the amount of adsorbent, contact time, and pH. The removal efficiency increased with the increase in contact time and adsorption dosage. The highest removal of TF-SCMNPs for Ni(II), Cu(II), and Cr(III) was obtained at pH 7, 10, and 10 during the contact time of 20 min, respectively. Adsorption data showed that it was better described by the Langmuir model for Ni(II) and Cu(II) and Freundlich model for Cr(III). The maximum adsorption capacity was estimated to be 4.476, 4.038, and 1.119 mg/g at optimum pH and room temperature for Cu(II), Ni(II), and Cr(III), respectively. The results show that the TF-SCMNPs can be used for the treatment of aqueous solutions containing heavy metals as an appropriate adsorbent in fast time with high efficiency.

Acknowledgments

This paper is issued from an integrated research of 93-03-27-25012 as a project number PhD student project of Mahsa Tahergorabi. Financial support was provided by Iran University of Medical Sciences, Iran.

References

[1] M.M. Zeitoun, E.-S.E. Mehana, Impact of water pollution with heavy metals on fish health: Overview and updates, Glob. Vet. 12 (2014) 219–231.

[2] M. Farzadkia, M. Gholami, M. Kermani, K. Yaghmaeian, Biosorption of hexavalent chromium from aqueous solutions by chemically modified brown algae of *Sargassum* sp. and dried activated sludge, Asian J. Chem. 24 (2012) 5257–5263.

[3] C.V. Mohod, J. Dhote, Review of heavy metals in drinking water and their effect on human health, Int. J. Innov. Res. Sci. Eng. Technol. 2 (2013) 2992–2996.

[4] X.-H. Zhao, F.-P. Jiao, J.-G. Yu, Y. Xi, X.-Y. Jiang, X.-Q. Chen, Removal of Cu(II) from aqueous solutions by tartaric acid modified multi-walled carbon nanotubes, Colloids Surf., A: Physicochem. Eng. Aspects 476 (2015) 35–41.

[5] B. Bina, M. Kermani, H. Movahedian, Z. Khazaei, Biosorption and recovery of copper and zinc from aqueous solutions by nonliving biomass of marine brown algae of *Sargassum* sp., Pak. J. Biol. Sci. 9 (2006) 1525–1530.

[6] M. Parmar, L.S. Thakur, Heavy metal Cu, Ni and Zn: Toxicity, health hazards and their removal techniques by low cost adsorbents: A short overview, Int. J. Plan. Environ. Sci. 3 (2013) 143–157.

[7] F. Fu, Q. Wang, Removal of heavy metal ions from wastewaters: A review, J. Environ. Manage. 92 (2011) 407–418.

[8] J. Duruibe, M. Ogwuegbu, J. Egwurugwu, Heavy metal pollution and human biotoxic effects, Int. J. Phys. Sci. 2 (2007) 112–118.

[9] M. Hua, S. Zhang, B. Pan, W. Zhang, L. Lv, Q. Zhang, Heavy metal removal from water/wastewater by nanosized metal oxides: A review, J. Hazard. Mater. 211–212 (2012) 317–331.

[10] J.-G. Yu, X.-H. Zhao, L.-Y. Yu, F.-P. Jiao, J.-H. Jiang, X.-Q. Chen, Removal, recovery and enrichment of metals from aqueous solutions using carbon nanotubes, JRNC 299 (2014) 1155–1163.

[11] J.-G. Yu, L.-Y. Yu, H. Yang, Q. Liu, X.-H. Chen, X.-Y. Jiang, X.-Q. Chen, F.-P. Jiao, Graphene nanosheets as novel adsorbents in adsorption, preconcentration and removal of gases, organic compounds and metal ions, Sci. Total Environ. 502 (2015) 70–79.

[12] H.K. Boparai, M. Joseph, D.M. O'Carroll, Kinetics and thermodynamics of cadmium ion removal by adsorption onto nano zerovalent iron particles, J. Hazard. Mater. 186 (2011) 458–465.

[13] M. Kumari, C.U. Pittman, D. Mohan, Heavy metals [chromium(VI) and lead(II)]. Removal from water using mesoporous magnetite (Fe_3O_4) nanospheres, J. Colloid Interface Sci. 442 (2015) 120–132.

[14] A. Mohagheghian, R. Vahidi-Kolur, M. Pourmohseni, J.-K. Yang, M. Shirzad-Siboni, Application of scallop SHELL-Fe_3O_4 nano-composite for the removal azo dye from aqueous solutions, Water Air Soil Pollut. 226 (2015) 1–16.

[15] G. Li, Z. Zhao, J. Liu, G. Jiang, Effective heavy metal removal from aqueous systems by thiol functionalized magnetic mesoporous silica, J. Hazard. Mater. 192 (2011) 277–283.

[16] Y. Shen, J. Tang, Z. Nie, Y. Wang, Y. Ren, L. Zuo, Preparation and application of magnetic Fe_3O_4 nanoparticles for wastewater purification, Sep. Purif. Technol. 68 (2009) 312–319.

[17] J.-F. Liu, Z.-S. Zhao, G.-B. Jiang, Coating Fe_3O_4 magnetic nanoparticles with humic acid for high efficient removal of heavy metals in water, Environ. Sci. Technol. 42 (2008) 6949–6954.

[18] W. Yantasee, C.L. Warner, T. Sangvanich, R.S. Addleman, T.G. Carter, R.J. Wiacek, G.E. Fryxell, C. Timchalk, M.G. Warner, Removal of heavy metals from aqueous systems with thiol functionalized superparamagnetic nanoparticles, Environ. Sci. Technol. 41 (2007) 5114–5119.

[19] M. Farrokhi, S.-C. Hosseini, J.-K. Yang, M. Shirzad-Siboni, Application of ZnO–Fe_3O_4 nanocomposite on the removal of azo dye from aqueous solutions: Kinetics and equilibrium studies, Water Air Soil Pollut. 225 (2014) 1–12.

[20] A. APHA, WEF (2005), Standard Methods for the Examination of Water and Wastewater, American Public Health Association, American Water Works Association, and Water Environment Federation, 2007.

[21] Y. Zhang, Q. Xu, S. Zhang, J. Liu, J. Zhou, H. Xu, H. Xiao, J. Li, Preparation of thiol-modified Fe_3O_4@SiO_2 nanoparticles and their application for gold recovery from dilute solution, Sep. Purif. Technol. 116 (2013) 391–397.

[22] A. Patterson, The Scherrer formula for X-ray particle size determination, Phys. Rev. 56 (1939) 978.

[23] J. Wang, S. Zheng, Y. Shao, J. Liu, Z. Xu, D. Zhu, Amino-functionalized Fe_3O_4@SiO_2 core–shell magnetic nanomaterial as a novel adsorbent for aqueous heavy metals removal, J. Colloid Interface Sci. 349 (2010) 293–299.

[24] C. Zhang, J. Sui, J. Li, Y. Tang, W. Cai, Efficient removal of heavy metal ions by thiol-functionalized superparamagnetic carbon nanotubes, Chem. Eng. J. 210 (2012) 45–52.

[25] S. Zhang, Y. Zhang, J. Liu, Q. Xu, H. Xiao, X. Wang, H. Xu, J. Zhou, Thiol modified Fe_3O_4@ SiO_2 as a robust, high effective, and recycling magnetic sorbent for mercury removal, Chem. Eng. J. 226 (2013) 30–38.

[26] O. Hakami, Y. Zhang, C.J. Banks, Thiol-functionalised mesoporous silica-coated magnetite nanoparticles for high efficiency removal and recovery of Hg from water, Water Res. 46 (2012) 3913–3922.

[27] R.K. Gautam, P.K. Gautam, S. Banerjee, S. Soni, S.K. Singh, M.C. Chattopadhyaya, Removal of Ni(II) by magnetic nanoparticles, J. Mol. Liq. 204 (2015) 60–69.

[28] N. Chiron, R. Guilet, E. Deydier, Adsorption of Cu(II) and Pb(II) onto a grafted silica: Isotherms and kinetic models, Water Res. 37 (2003) 3079–3086.

[29] M.A. Khraisheh, Y.S. Aldegs, W.A. Mcminn, Remediation of wastewater containing heavy metals using raw and modified diatomite, Chem. Eng. J. 99 (2004) 177–184.

[30] X.-J. Tong, J.-Y. Li, J.-H. Yuan, R.-K. Xu, Adsorption of Cu(II) by biochars generated from three crop straws, Chem. Eng. J. 172 (2011) 828–834.

[31] J.C. Moreno, R. Gómez, L. Giraldo, Removal of Mn, Fe, Ni and Cu ions from wastewater using cow bone charcoal, Materials 3 (2010) 452–466.

[32] M. Samarghandi, S. Azizian, M.S. Siboni, S. Jafari, S. Rahimi, Removal of divalent nickel from aqueous solutions by adsorption onto modified holly sawdust: Equilibrium and kinetics, J. Environ. Health Sci. Eng. 8 (2011) 167–174.
[33] M. Shirzad-Siboni, A. Khataee, A. Hassani, S. Karaca, Preparation, characterization and application of a CTAB-modified nanoclay for the adsorption of an herbicide from aqueous solutions: Kinetic and equilibrium studies, C.R, Chim 18 (2015) 204–214.
[34] M. Matouq, N. Jildeh, M. Qtaishat, M. Hindiyeh, M.Q. Al Syouf, The adsorption kinetics and modeling for heavy metals removal from wastewater by Moringa pods, J. Environ. Chem. Eng. 3 (2015) 775–784.
[35] A. Gholizadeh, M. Kermani, M. Gholami, M. Farzadkia, Kinetic and isotherm studies of adsorption and biosorption processes in the removal of phenolic compounds from aqueous solutions: Comparative study, J. Environ. Health Sci. Eng. 11 (2013) 11–29.
[36] A. Gholizadeh, M. Kermani, M. Gholami, M. Farzadkia, K. Yaghmaeian, Removal efficiency, adsorption kinetics and isotherms of phenolic compounds from aqueous solution using rice bran ash, Asian J. Chem. 25 (2013) 3871–3878.
[37] Q. Wu, R. You, Q. Lv, Y. Xu, W. You, Y. Yu, Efficient simultaneous removal of Cu(II) and $Cr_2O_7^{2-}$ from aqueous solution by a renewable amphoteric functionalized mesoporous silica, Chem. Eng. J. 281 (2015) 491–501.
[38] B. Guo, F. Deng, Y. Zhao, X. Luo, S. Luo, C. Au, Magnetic ion-imprinted and–SH functionalized polymer for selective removal of Pb(II) from aqueous samples, Appl. Surf. Sci. 292 (2014) 438–446.
[39] X. Liang, Y. Xu, G. Sun, L. Wang, Y. Sun, X. Qin, Preparation, characterization of thiol-functionalized silica and application for sorption of Pb^{2+} and Cd^{2+}, Colloids Surfaces A: Physicochem. Eng. Aspects 349 (2009) 61–68.
[40] Z.A. Alothman, A.W. Apblett, Metal ion adsorption using polyamine-functionalized mesoporous materials prepared from bromopropyl-functionalized mesoporous silica, J. Hazard. Mater. 182 (2010) 581–590.
[41] L. Tang, Y. Fang, Y. Pang, G. Zeng, J. Wang, Y. Zhou, Y. Deng, G. Yang, Y. Cai, J. Chen, Synergistic adsorption and reduction of hexavalent chromium using highly uniform polyaniline–magnetic mesoporous silica composite, Chem. Eng. J. 254 (2014) 302–312.
[42] R. Katal, E. Hasani, M. Farnam, M.S. Baei, M.A. Ghayyem, Charcoal ash as an adsorbent for Ni(II) adsorption and its application for wastewater treatment, J. Chem. Eng. Data 57 (2012) 374–383.
[43] K.G. Bhattacharyya, S.S. Gupta, Adsorption of a few heavy metals on natural and modified kaolinite and montmorillonite: A review, Adv. Colloid Interface Sci. 140 (2008) 114–131.
[44] H.V. Tran, L. Dai Tran, T.N. Nguyen, Preparation of chitosan/magnetite composite beads and their application for removal of Pb(II) and Ni(II) from aqueous solution, Mater. Sci. Eng. C 30 (2010) 304–310.
[45] Y. Ho, C. Huang, H. Huang, Equilibrium sorption isotherm for metal ions on tree fern, Process Biochem. 37 (2002) 1421–1430.
[46] E. López, B. Soto, M. Arias, A. Núñez, D. Rubinos, M. Barral, Adsorbent properties of red mud and its use for wastewater treatment, Water Res. 32 (1998) 1314–1322.
[47] K.G. Bhattacharyya, S.S. Gupta, Influence of acid activation on adsorption of Ni(II) and Cu(II) on kaolinite and montmorillonite: Kinetic and thermodynamic study, Chem. Eng. J. 136 (2008) 1–13.
[48] R. Vieira, E. Guibal, E. Silva, M. Beppu, Adsorption and desorption of binary mixtures of copper and mercury ions on natural and crosslinked chitosan membranes, Adsorption 13 (2007) 603–611.
[49] M. Arias, M. Barral, J. Mejuto, Enhancement of copper and cadmium adsorption on kaolin by the presence of humic acids, Chemosphere 48 (2002) 1081–1088.
[50] M.E. Argun, Use of clinoptilolite for the removal of nickel ions from water: Kinetics and thermodynamics, J. Hazard. Mater. 150 (2008) 587–595.